

Discovery of a Transient X-Ray Pulsar, AX J1841.0–0536, in the Scutum Arm Region with ASCA

Aya BAMBA, Jun YOKOGAWA, Masaru UENO, and Katsuji KOYAMA

Department of Physics, Graduate School of Science, Kyoto University, Sakyo-ku, Kyoto 606-8502

bamba@cr.scphys.kyoto-u.ac.jp, jun@cr.scphys.kyoto-u.ac.jp, masaru@cr.scphys.kyoto-u.ac.jp, koyama@cr.scphys.kyoto-u.ac.jp
and

Shigeo YAMAUCHI

Faculty of Humanities and Social Sciences, Iwate University, 3-18-34 Ueda, Morioka, Iwate 020-8550

yamauchi@hiryu.hss.iwate-u.ac.jp

(Received 2001 June 19; accepted 2001 September 12)

Abstract

We report on the discovery of a transient X-ray pulsar, AX J1841.0–0536, serendipitously found in the Scutum arm region with the ASCA in two separate observations. The X-ray flux is very faint at the beginning, but exhibits two flares in the second observation. The flare flux increases by a factor 10 within only ~ 1 hr. Coherent pulsations with a period of 4.7394 ± 0.0008 s were detected in the brightest flare phase. The X-ray spectra in the quiescent and flare phases were fitted with an absorbed power-law model with a photon index ~ 1 plus a narrow Gaussian line at the center energy of 6.4 keV. The interstellar column density of $\sim 3 \times 10^{22} \text{ cm}^{-2}$ may indicate that AX J1841.0–0536 is located at a tangential point of the Scutum arm at ~ 10 kpc distance. The coherent pulsations, large flux variability and the spectral shape suggest that AX J1841.0–0536 is a Be/X-ray binary pulsar.

Key words: stars: neutron — stars: pulsars: individual (AX J1841.0–0536) — X-rays: spectra — X-rays: stars — X-rays: transient

1. Introduction

The Scutum region near $l \sim 30^\circ$ is in the tangential line of sight of a galactic arm (the Scutum arm), and hence shows intensity excesses in the infrared, radio and γ -ray regions (e.g., Hayakawa et al. 1977) as well as diffuse X-rays (Yamauchi, Koyama 1993; Sugizaki et al. 2001). This region is also rich in X-ray binary sources; many transient X-ray sources have also been discovered (e.g., Koyama et al. 1990; Yamauchi et al. 1995; Terada et al. 1999). From the spectral and flux variability, these X-ray transients are suspected to be either neutron-star binaries with high mass or low-mass stars, or black-hole binaries (Tanaka, Shibazaki 1996). Coherent X-ray pulsations have been found from some of them, suggesting Be/X-ray binaries.

Among them, an unusual source is AX 1845.0–0433, which exhibited violent flares with a very rapid rise time of $\lesssim 10^4$ s (Yamauchi et al. 1995). Apart from the unusual flares, other characteristics are similar to those of high-mass X-ray binaries. In fact, Coe et al. (1996) reported an O9.5 star as the optical counterpart of AX 1845.0–0433. Nevertheless, no coherent pulsation has been found.

In the ASCA survey and pointing observations on the Scutum arm region, we found another unusual source, AX J1841.0–0536, which also exhibited violent and rapid flares (Bamba, Koyama 1999). This paper reports on a detailed analysis of this new transient X-ray source, particularly on the detection of coherent pulsations and phase resolved spectral analyses.

2. Observations and Data Reduction

The first ASCA observation of a region around $(l, b) = (26.9, -0.1)$ was made on 1994 April 12, or MJD 49454.677–49454.701, as a part of the Scutum arm survey project (hereinafter, obs. 1). A longer exposure follow-up observation was made on 1999 October 3–4, or on MJD 51454.252–51455.463 (obs. 2). ASCA carried four XRTs (X-Ray Telescopes, Serlemitsos et al. 1995) with two GISs (Gas Imaging Spectrometers, Ohashi et al. 1996) and two SISs (Solid-state Imaging Spectrometers, Burke et al. 1994) on the focal planes. Since our target was out of the SIS field in both observations, we do not refer to the SIS in this paper. The GISs were operated in the nominal PH mode with a time resolution of 62.5 ms (High bit-rate) or 0.5 s (Medium bit-rate).

We rejected the GIS data obtained in the South Atlantic Anomaly, in low cut-off rigidity regions (< 6 GV), or when the target's elevation angle was low ($< 5^\circ$). Particle events were removed by the rise-time discrimination method (Ohashi et al. 1996). After these screenings, the total available exposure times of obs. 1 and 2 were ~ 2 ks and ~ 36 ks, respectively. To increase the statistics, the data of the two detectors, GIS-2 and GIS-3, were combined in a following study.

3. Results

3.1. X-Ray Image

A transient source is found in both obs. 1 and obs. 2. Figure 1 shows a point-like source image located near the galactic plane. The source position is determined by the method of Gotthelf et al. (2000) and is (R.A., Dec.)_{J2000} = (18^h41^m50^s.2, −05°36′00″) with an uncertainty of $\sim 1'$. Therefore, we designate this source as AX J1841.0–0536 (this source was at first named AX J1841.0–0535.8 based on less-accurate positioning; Bamba, Koyama 1999). No X-ray source has been found within the error region in the SIMBAD database.¹ However, this source is in an error region ($0.4 \times 4^\circ$) of a previous X-ray transient (the Ginga source No. 2 in Koyama et al. 1990).

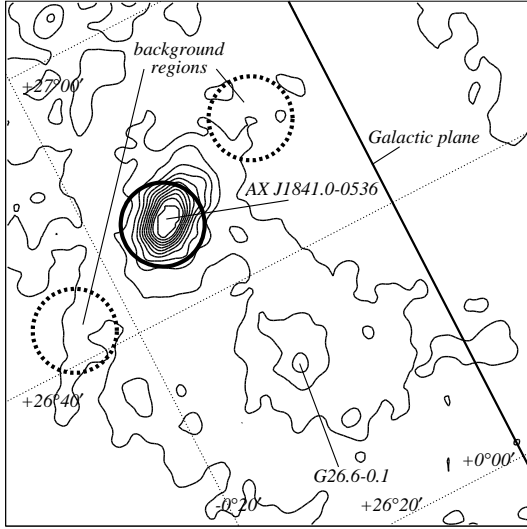


Fig. 1. X-ray image around AX J1849.8–0530 in the 2.0–7.0 keV band combined with both observations, with the galactic coordinates. G26.6–0.1 is an unidentified hard diffuse source (A. Bamba et al. unpublished). The source and background regions for the spectral and timing analyses are also indicated by the solid and dotted circles, respectively.

3.2. Light Curve and Timing Analyses

The light curves of AX J1841.0–0536 in both observations are shown in figure 2. The X-ray flux is highly variable with two flares of the on-set epochs at MJD 51454.7 and MJD 51455.3 with an interval of only ~ 0.6 d. As can be seen in figure 2, the flares are found in the hard bands, while the soft band fluxes are essentially constant. A remarkable fact is that the on-set time of both the flares are extremely rapid; the fluxes increased by one order of magnitude within 1 hr.

To study the time evolution, we divided obs. 2 into three epochs: obs. 2a (MJD 51454.252–51454.700), obs. 2b (MJD 51454.700–51455.300), and obs. 2c (MJD 51455.300–51455.463), as shown in figure 2. We then performed detailed timing analyses of the brightest flare

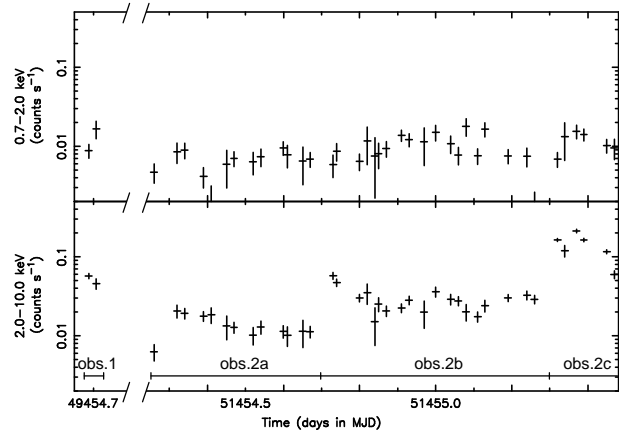


Fig. 2. X-ray light curves of AX J1841.0–0536 observed with GIS-2 and GIS-3 (bin time = 1600 s) in obs. 1 and obs. 2. The upper and lower panels are those in the 0.7–2.0 keV and 2.0–10.0 keV bands, respectively. For the spectral analyses (see text), obs. 2 was divided into three epochs (obs. 2a, obs. 2b, and obs. 2c), as indicated in the lower panel.

episode (obs. 2c). We extracted ~ 1000 photons, including ~ 90 background photons, in the 1.9–4.9 keV band from a $3'$ radius circle around the source (the solid circle in figure 1), corrected the photon arrival times to those at the barycenter and applied an FFT (Fast Fourier Transform) algorithm. The resulting power-density spectrum, figure 3 (left), shows a peak at ~ 0.211 Hz. With 13471 frequencies examined, the chance probability of producing such a large peak is $\sim 9.8 \times 10^{-6}$, and hence the 0.211 Hz oscillation is highly significant. We next performed an epoch-folding search and determined a more accurate pulse period of $P = 4.7394 \pm 0.0008$ s. Figure 3 (right) shows the folded pulse profile in the soft (1.9–4.9 keV) and hard (4.9–10.0 keV) bands.

The pulse shapes are sinusoidal in both energy bands, but the background-subtracted pulse fraction is larger in the soft (28%) band than in the hard (8%) band. Although same analyses, FFT and epoch folding, were performed for the other data sets, no significant power was found with the 3σ upper limit of the background-subtracted pulse fraction in the soft band of about 45% and 12% for obs. 2a and 2b, respectively.

3.3. Spectral Analyses

We made time-sliced X-ray spectra using photons from the same region of the timing analysis (in the $3'$ radius circle around the source; see figure 1). The contribution of the galactic ridge emission is not negligible for AX J1841.0–0536 located closely on the galactic plane at $(l, b) = (26.7, 0.1)$. Contamination from an unidentified hard diffuse source G26.6–0.1 (A. Bamba et al. unpublished) and vignetting may not be ignored. We thus made the background spectrum by adding data from two

¹ see <http://simbad.u-strasbg.fr/sim-fid.pl>.

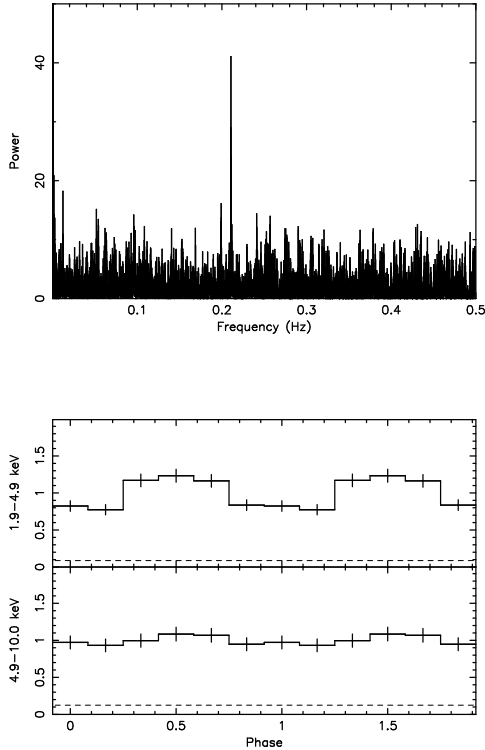


Fig. 3. Upper panel: Power-density spectrum in obs. 2c. A significant peak is detected around ~ 0.211 Hz. Lower panel: Pulse profiles in the 1.9–4.9 keV (upper panel) and the 4.9–10.0 keV (lower panel) bands in obs. 2c. The vertical axes indicate the normalized intensity per bin. The horizontal axis indicates the pulsation phase and the epoch of the beginning of the phase corresponds to MJD 51455.300. The background levels are indicated by the broken lines.

source-free regions, indicated by the dotted-circles in figure 1. These two regions were selected to compensate for the latitude-dependent galactic ridge emission (Kaneda et al. 1997) and contamination of G26.6–0.1. The vignetting is also the same as the source region.

The background-subtracted spectrum in the brightest flare phase (the second flare, or obs. 2c) was at first fitted with a power-law function. The absorption column was estimated from the cross sections of Morrison and McCammon (1983) with solar abundances. Although this model is statistically acceptable, we see a systematic data excess at around 6–7 keV. Adding a narrow Gaussian line to the model reduced the χ^2 from 51.2/52 to 43.2/50 ($\chi^2/\text{degree of freedom}$); thus, the presence of the line is significant. The center energy of the line is 6.40 ± 0.12 keV (hereinafter, the errors are of 90% confidence level, unless otherwise mentioned), implying that the line is due to neutral or low-ionized irons.

An absorbed thin-thermal plasma model fitting, on the other hand, requires unrealistically high temperature of > 80 keV, and is hence unlikely.

We then fit the background-subtracted spectra of the other epochs with a power-law plus a Gaussian model,

fixing the center energy of the line to be 6.40 keV (the best-fit value in obs. 2c). These fittings are acceptable for all epochs. The spectra and the best-fit models for the four separate epochs are shown in figure 4, while the best-fit parameters are listed in table 1.

4. Discussion

AX J1841.0–0536 is in the error region ($l = 26.6 \pm 0.2^\circ, b = -0.5 \pm 2.0^\circ$) of a previous X-ray transient No. 2 in Koyama et al. (1990). Although the position uncertainty is large, the X-ray features, power-law index of 1.5 ± 0.3 , flux of 2×10^{-11} erg cm $^{-2}$ s $^{-1}$ and $\log(N_{\text{H}})$ of 22.7 ± 0.3 are similar to those of AX J1841.0–0536 in obs. 1 and obs. 2b. Therefore these two transients are likely to be the same source. From the flux history, we suspect that the quiescent level of AX J1841.0–0536 is on the order of 2×10^{-12} erg cm $^{-2}$ s $^{-1}$, and that flares may occur very frequently. More bright flares of a level of 10^{-10} erg cm $^{-2}$ s $^{-1}$ are, however not frequent.

Although the limited statistics allows a constant-value hypothesis of N_{H} , we see a hint that N_{H} increase with increasing flux, which suggests that the circum-stellar absorption becomes larger in the flare, due to the larger gas accretion. Therefore, the interstellar absorption should be regarded as the minimum value of $\sim 3.2^{+6.2}_{-2.4} \times 10^{22}$ cm s $^{-1}$ (obs. 1 and obs. 2a). The large error of N_{H} does not allow us to reliably estimate the source distance. Nevertheless, we simply estimate the distance to AX J1841.0–0536 to be 1–10 kpc, assuming the average density in the galactic plane to be 1 H cm $^{-3}$. This value is consistent with that the transient source is located in the tangential point of the Scutum arm.

Koyama et al. (1990) reported many X-ray transient sources in the Scutum arm with a flare of the order of 10^{36} erg s $^{-1}$, and suggested that most are Be/X-ray binaries. Since the hard X-ray spectrum, neutral iron line, erratic flux variability and coherent pulsations are characteristic of Be/X-ray binaries, AX J1841.0–0536 would be a member of this sub-class of X-ray pulsars. No optical counterpart has been found to confirm this classification. The luminosity is consistent with that of a “Type I outburst” of Be/X-ray binaries (Negueruela 1998).

From a semi-empirical relation of the orbital period vs. pulse period and the X-ray luminosity (Corbet 1984; Corbet et al. 1999), we suggest that the orbital period of AX J1841.0–0536 is ~ 25 days. Be/X-ray binaries often exhibit flares with an interval of the orbital period (c.f. 4U 1223–62, Watson et al. 1982; V 0332+53, Stella et al. 1985) due to a gas surge during passage near to the peri-astron or across the equatorial plane. From AX J1841.0–0536, we observed two subsequent flares separated by ~ 0.6 d, which is much shorter than not only the predicted orbital period, but also the shortest orbital period known for a Be/X-ray binary pulsar, 16.7 days for A0538–66 (Corbet et al. 1997).

Parmar et al. (1989) reported that quasi-periodic flares with a 3.96 hr interval in the limited episode of a Be/X-ray binary EXO 2030+375, which has spin and orbital peri-

Table 1. Best-fit parameters for AX J1841.0–0536 for an absorbed power-law and a Gaussian model.*

Parameters	obs. 1	obs. 2a	obs. 2b	obs. 2c
Power-law				
Γ	1.0 (0.3–1.9)	2.0 (0.9–3.6)	0.7 (0.1–1.3)	1.1 (0.9–1.4)
Gaussian				
Center (keV).....	6.4 (fixed)	6.4 (fixed)	6.4 (fixed)	6.4 (6.3–6.5)
$EW^\dagger (\times 10^2 \text{ eV})$	(< 4.7)	not determined	1.9 (< 4.3)	2.3 (1.0–3.8)
$N_H^\ddagger (\times 10^{22} \text{ cm}^{-2})$	3.2 (1.1–6.4)	3.2 (0.8–8.4)	4.3 (2.0–7.9)	7.2 (6.0–8.6)
Flux $^\S (\text{erg cm}^{-2} \text{ s}^{-1})$	2.0×10^{-11}	1.9×10^{-12}	1.3×10^{-11}	9.5×10^{-11}
Luminosity $^{\S\P} (\text{erg s}^{-1})$	2.3×10^{35}	2.3×10^{34}	1.5×10^{35}	1.1×10^{36}
$\chi^2/\text{d.o.f}^\#$	13.2/21	15.1/13	41.9/34	43.2/50

* Errors and upper limits are at 90% confidence for one relevant parameter.

† Equivalent width.

‡ Assuming the solar abundance ratio (Morrison, McCammon 1983).

§ Estimated in the 2.0–10.0 keV band.

¶ Assumed distance is 10 kpc (see section 4.)

$^\#$ Degree of freedom.

ods of ~ 42 s and 46.0 day respectively (Stollberg 1997), are both different from the flare interval. They inferred that the quasi-periodic rapid flares, fast rise and exponential decay, are due to instabilities in the either magnetosphere (e.g., Lamb et al. 1977) or the accretion disk (e.g., Taam, Lin 1984). Asymmetric flow of a stellar wind (e.g., Taam, Fryxell 1988), or non-homogeneity of the OB star wind (e.g., Baade 1984) may also be a possible scenario. The same process can be applied to the two flares of AX J1841.0–0536, although the detailed structure, the flare profile, number, size and so on are significantly different from those of EXO 2030+375.

A remarkable feature of AX J1841.0–0536 is an eruptive on-set of a flare with a rise-time of ~ 1 hour. We note that other transient sources, AX J1845.0–0433 (Yamauchi et al. 1995) and XTE J1739–302 (Smith et al. 1998; Sakano et al. 2001), exhibit multiple flares with a fast-rise of a few hours, although no coherent pulsation has been found. We suspect that these new transients comprise a new sub-class of X-ray binaries, which provides a crucial test for the accretion-flow instability. Therefore, further monitor observations on these unusual X-ray binaries are encouraged.

We thank all of the ASCA galactic ridge survey members. This research made use of the SIMBAD database, operated at CDS, Strasbourg, France. We also thank an anonymous referee, D. Yonetoku and K. Imanishi for their useful comments and suggestions. A.B. and J.Y. are supported by JSPS Research Fellowship for Young Scientists.

References

- Baade, D. 1984, *A&A*, 135, 101
 Bamba, A., & Koyama, K. 1999, *IAU Circ.*, 7324
 Burke, B.E., Mountain, R.W., Daniels, P.J., Dolat, V.S., & Cooper, M.J. 1994, *IEEE Trans. Nucl. Sci.*, 41, 375
 Coe, M.J., Fabregat, J., Negueruela, I., Roche, P., & Steele, I.A. 1996, *MNRAS*, 281, 333
 Corbet, R.H.D. 1984, *A&A*, 141, 91
 Corbet, R.H.D., Charles, P.A., Southwell, K.A., & Smale, A.P. 1997, *ApJ*, 476, 833
 Corbet, R.H.D., Marshall, F.E., Peele, A.G., & Takeshima, T. 1999, *ApJ*, 517, 956
 Gotthelf, E.V., Ueda, Y., Fujimoto, R., Kii, T., & Yamaoka, K. 2000, *ApJ*, 543, 417
 Hall, T.A., Finley, J.P., Corbet, R.H.D., & Thomas, R.C. 2000, *ApJ*, 536, 450
 Hayakawa, S., Itoh, K., Matsumoto, T., & Uyama, K. 1977, *A&A*, 58, 325
 Kaneda, H., Makishima, K., Yamauchi, S., Koyama, K., Matsuzaki, K., & Yamasaki, N.Y. 1997, *ApJ*, 491, 638
 Koyama, K., Kawada, M., Kunieda, H., Tawara, Y., Takeuchi, Y., & Yamauchi, S. 1990, *Nature*, 343, 148
 Lamb, F.K., Fabian, A.C., Pringle, J.E., & Lamb, D.Q. 1977, *ApJ*, 217, 197
 Morrison, R., & McCammon, D. 1983, *ApJ*, 270, 119
 Negueruela, I. 1998, *A&A*, 338, 505
 Ohashi, T., Ebisawa, K., Fukazawa, Y., Hiyoshi, K., Horii, M., Ikebe, Y., Ikeda, H., Inoue, H., et al. 1996, *PASJ*, 48, 157
 Parmar, A.N., White, N.E., Stella, L., Izzo, C., & Ferri, P. 1989, *ApJ*, 338, 359
 Sakano, M., Koyama, K., Murakami, H., Maeda, Y., & Yamauchi, S. 2001, *ApJS*, submitted
 Serlemitsos, P.J., Jalota, L., Soong, Y., Kunieda, H., Tawara, Y., Tsusaka, Y., Suzuki, H., Sakima, Y., et al. 1995, *PASJ*, 47, 105
 Smith, D.M., Main, D., Marshall, F., Swank, J., Heindl, W.A., Leventhal, M., in't Zand, J.J.M., & Heise, J. 1998, *ApJL*, 501, L181
 Stella, L., White, N.E., Davelaar, J., Parmar, A.N., Blissett, R.J., & van der Klis, M. 1985, *ApJ*, 288, L45
 Stollberg, M.T. 1997, PhD Thesis, University Alabama
 Sugizaki, M., Mitsuda, K., Kaneda, H., Matsuzaki, K., Yamauchi, S., & Koyama, K. 2001, *ApJS*, 134, 77
 Taam, R.E., & Lin, D.N.C. 1984, *ApJ*, 287, 761
 Taam, R.E., & Fryxell, B.A. 1988, *ApJ*, 327, L73
 Tanaka, Y., & Shibazaki, N. 1996, *ARA&A*, 34, 607
 Terada, Y., Kaneda, H., Makishima, K., Ishida, M., Matsuzaki, K., Nagase, F., & Kotani, T. 1999, *PASJ*, 51, 39

Watson, M.G., Warwick, R.S., & Corbet, R.H.D. 1982, MNRAS, 199, 915

Yamauchi, S., Aoki, T., Hayashida, K., Kaneda, H., Koyama, K., Sugizaki, M., Tanaka, Y., Tomida, H., & Tsuboi, Y. 1995, PASJ, 47, 189

Yamauchi, S., & Koyama, K. 1993, ApJ, 404, 620

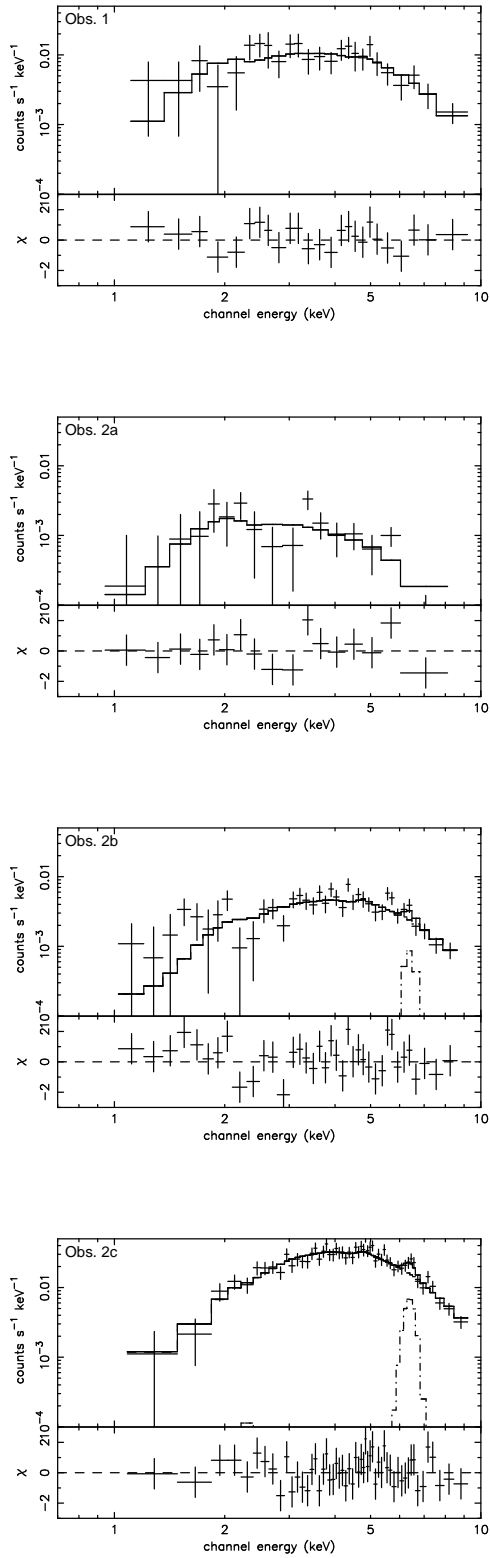


Fig. 4. Background-subtracted spectra (crosses) and the best-fit models (solid histograms). Data residuals are shown in the lower panel of each figure.